Some Electronic Correlation Effects in the Topological Analysis of the Laplacian of the Electronic Charge Density in C-*n*-Butonium Cations

Rosana M. Lobayan,[†,‡] Gladis L. Sosa,[‡] Alicia H. Jubert,*[,§] and Nélida M. Peruchena[‡]

Departamento de Física and Lab. Estructura Molecular y Propiedades, Área de Química Física, Facultad de Ciencias Exactas y Naturales y Agrimensura, UNNE, Avda. Libertad 5460, (3400) Corrientes, Argentina, and CEQUINOR (CONICET, UNLP), Departamento de Química, Facultad de Ciencias Exactas y Facultad de Ingeniería, UNLP.,C.C. 962, Calle 47 y 115 (1900) La Plata, Argentina

Received: July 7, 2004; In Final Form: October 22, 2004

In this work, we present a topological study of the Laplacian of the electronic density using a 6-311++G** basis set, at Hartree−Fock (HF) and second-order Møller−Plesset (MP2) (full-electron and frozen-core) levels of theory, for the carbocations 2-C-*n*-butonium generated upon the insertion of a proton into the secondary C−C bond during the protonation of *n*-butane. The charge concentration, CC, critical points of the Laplacian distribution at each valence shell, VS, of carbon atoms, and the charge concentration closer to hydrogen atoms are studied. Also, the bonding critical points of the electronic density are analyzed. We analyze some effects that Coulomb correlation has on topological features of the electronic distribution. It is shown that they are mainly reflected in a decreasing of the charge concentrations at the VS and in a contraction of the VS to the nuclei. They are more pronounced over C−C bonds than in C−H bonds. The sensitivity of some parameters derived from this topological analysis to the correlation effect of core electrons and subtle effects related to hyperconjugative interactions are shown. Some consequences of different schemes (double and triple split-valence basis set with diffuse and polarization functions) in the definition of subtle VS charge concentrations at 3c-2e bond paths are presented. It is also demonstrated here how the facts that allow us to understand the MP2 stability order found in the carbocationic species 2-C-*n*-butonium > 1-C-*n*-butonium > 2-H-*n*-butonium > 1-H-*n*-butonium are similarly depicted at correlated and uncorrelated levels of calculation.

Introduction

Carbonium ions are formed by the insertion of a proton into C−C or C−H bonds and present one characteristic three-center-two-electron bond (3c-2e). They are important species involved in acid-catalyzed alkane transformations. The methonium[1] (CH_5^+) and ethonium[2] ($C_2H_7^+$) ions are the smallest members of this family and have already been observed in the gas phase by spectroscopic methods.[3,4] They have also been mostly studied by theoretical methods.[5,6] The use of ab initio calculations, particularly those including electron correlation effects, have proven to provide excellent predictions for the equilibrium energy and geometry of these carbocations.

Esteves et al. have performed ab initio calculations for the proponium,[7] isobutonium,[8] and the *n*-butonium[9a,b] cations, at the perturbational second- and fourth-order Møller−Plesset levels of theory. For the *i*-$C_4H_{11}^+$, the protonated isobutane, the calculations indicated that van der Waals complexes between *tert*-butyl carbenium ion and hydrogen and isopropyl carbenium ion and methane have a lower energy than carbonium ions themselves. Indeed, additional calculations[9b] revealed that the decomposition of 2-H-isobutonium, hypothetically formed through the protonation of the tertiary C−H bond of isobutane, and C-isobutonium, formed upon protonation of the C−C bond of isobutane, to the respective van der Waals complexes occurs with low or no activation energy at all. Collins and O'Malley found a similar conclusion using DFT calculations.[10]

Protonation of *n*-butane can take place at the primary or secondary C−H bonds, (1-H-*n*-butonium and 2-H-*n*-butonium) and at two different types of C−C bonds, external or internal, denoted 1-C-*n*-butonium and 2-C-*n*-butonium, respectively, to form different isomeric structures of the *n*-butonium cations (*n*-$C_4H_{11}^+$). The stability of these carbonium ions decreases in the order

2-C-*n*-butonium > 1-C-*n*-butonium > 2-H-*n*-butonium > 1-H-*n*-butonium

The protonation over C−C bonds is shown in Scheme 1.

If one takes into consideration that the *i*-$C_4H_{11}^+$ cations are isomeric to the *n*-$C_4H_{11}^+$ cations, a direct comparison of energy between them is possible. Consequently, Esteves et al. have proposed the following σ-basicity scale[11] on the basis of the relative stability of the carbocations:

C−C > *tert*-C−H > *sec*-C−H > primary C−H > CH_4

This scale differs slightly from the one proposed by Olah,[12] related to the reactivity of the σ-bond. However, it must be taken into consideration that the Esteves scale is related to the thermodynamics of the protonation of the σ-bond, reflecting the basicity of the bonds.

In previous works,[13,14] we analyzed the topology of the distribution of the charge density in protonated species of *n*-butane and *i*-butane and their van der Waals complexes; this analysis has been used in order to establish a relationship among the parameters that determine the stability order found for the different species and relate them to the structure of the

[†] Departamento de Física.
[‡] Lab. Estructura Molecular y Propiedades, Área de Química Física.
[§] CEQUINOR (CONICET, UNLP), Departamento de Química.

10.1021/jp0469923 CCC: $30.25
Published on Web 12/14/2004

SCHEME 1. Hypothetical Protonation over Nonequivalent C−C Bonds in *n*-Butane, Leading to the Different C-*n*-Butonium Cations

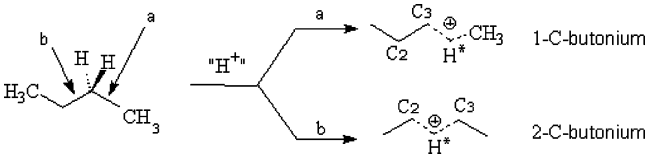

carbonium ions. We found that a better understanding of the relative stability of the protonated species of *n*-butane and *i*-butane is obtained when the topological properties at the bond critical points on the distribution of the electronic charge density in the 3c-2e bonds are considered. A 3c-2e bond of the C−H*−H* type is found in all of the H-*n*-butonium cations (six, overall), and also, a 3c-2e bond of the C−H*−C type is found in all of the C-*n*-butonium cations (five, overall). These studies shown that the stability of the protonated species, both C-*n*-butonium and H-*n*-butonium cations, depends fundamentally on the way in which the charge of the cation is delocalized around the 3c-2e bonds. In these works, we concluded that in H-*n*-butonium cations, the stabilization degree is related to an increase of the electronic density between the H* atoms and at the H*−H* bond and to a decrease of the density between the H* and C atoms involved in the three-centered bond. These facts are accompanied by a shortening of the H*−H* bond, a lengthening of the C−H* distance, and a decrease of the H*−C−H* angle.

After analyzing the topology of the distribution of the charge density in all C-butonium cations, we have found indicators of the delocalization of electron charge density on the atoms involved in the three-centered bond and in the remaining fragments. This delocalization of the density on the C−H* bonds and neighboring C−X bonds (with X = C, H) is higher in C_{sec}−H*−C_{sec} than in C_{prim}−H*−C_{sec} in C-*n*-butonium cations, but lower than the delocalization that occurs in C_{ter}−H*−C_{met} at the C-*i*-butonium cation. Thus, from topological considerations taking over the electronic charge density function, the stability order is

$$C_{tertiary} > C_{secondary} > C_{primary}$$

These results agree with the idea that these species achieve their stabilization through the distribution of the positive charge of the proton onto the σ-bonds.[14]

In a recent work,[15] a systematic HF/6-311++G** study of the topology of the Laplacian of the electronic density for the isomeric structures of the *n*-butonium cations was done. This allowed us to visualize the changes that operate on the distribution of the electronic density, depending on the protonation site of the hydrocarbon. This type of study is frequently employed to detect nucleophilic and electrophilic attack sites, analyzing (3, +1) and (3, +3) critical points. We have demonstrated how this methodology, analyzing (3, −3) critical points, could also be used to obtain deeper insights related to displacement effects of the electronic density through the σ-bonds, delocalization of the positive charge, and degree of electronic deficiency of the C atom, thus allowing the understanding of the stability order found among the C-*n*-butonium and H-*n*-butonium. These results were consistent with the basicity scale proposed by Esteves et al.[11] The aim of this work is, given the MP2 structures, to examine the role of electron correlation in the topological description of the electronic distribution of these carbocationic systems. We present here the results derived from a study of the topology of the Laplacian of the electronic charge density for two conformers of 2-C-*n*-butonium cations (see Figure 1) at Hartree−Fock (HF) and full-electron and frozen-core second-order Møller−Plesset (MP2) levels of calculation using double and triple split-valence basis set schemes of contraction, adding polarization and diffuse functions to carbon and hydrogen atoms.

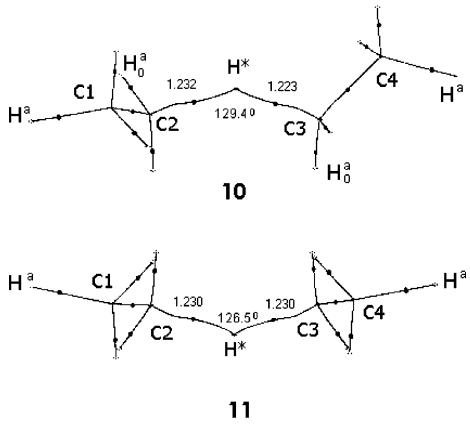

Figure 1. Molecular graphs of 2-C-*n*-butoniums (**10** and **11**). The bond critical points (obtained from topological analysis of the electronic density) are denoted by filled circles. H* represents the incoming proton. H_0 represents the H atoms located on the protonated C (C(H*)). With H^a or $H_0{}^a$, we distinguish the C−H bonds trans to C−H* or C−H bonds, respectively. Also are displayed the relevant geometrical parameters.

AIM Theory

The objective of the theory of atoms in molecules (AIM), developed by Bader et al.,[16,17] is extracting chemical insights from modern ab initio wave functions. This was extensively applied to study different chemical properties.[18−26] The topological properties of electronic density distribution, $\rho(r)$,[16] are used for the characterization of chemical bonds in a molecular system. The topological features of the Laplacian of electronic density distribution, $\nabla^2\rho(r)$, are powerful tools in the interpretation of quantum chemical results, because they provide an enhanced view of the local form of the electronic density. This type of analysis was useful to study the structure and geometry of hydrogen-bonded complexes,[27] to predict the sites of electrophilic and nucleophilic attack and their relative reactivities,[28−30] to detect differential delocalization/localization of lone pairs,[31] and to predict and understand biochemical processes and catalysis phenomena.[32−35] The full topology of the Laplacian in small molecules was also recently explored.[36,37]

The local maxima or charge concentrations (CCs) displayed by $-\nabla^2\rho(r)$ have been shown to yield a faithful mapping of localized electron domains that are assumed to be present in the valence shell of a central atom in the VSEPR (valence shell electronic pair repulsion) model[38,39] of molecular geometry, providing a physical basis for this model.[40,41] The correspondence between the critical points (CPs) of the Laplacian and the electron pairs in the VSEPR model was the subject of recent studies.[42−47] Another successful model, the LCP (ligand closed packing) model,[48] is also based on a huge number of experimental observations, which find their physical basis in AIM. This model is essentially equivalent to the VSEPR model, but explicitly recognizes the importance of intramolecular interactions between adjacent nonbonded atoms.

Bonding or nonbonding localized pairs of electrons are evident in the topology of $-\nabla^2\rho(r)$ and in another one-electron density function: the electron localization function (ELF).[49] The

topology of this function is homeomorphic to $-\nabla^2\rho(r)$ with few exceptions. However, it is worth stressing that the pattern of maxima in $-\nabla^2\rho(r)$ is superior in recovering the classical Lewis model because $-\nabla^2\rho(r)$ corresponds more closely to the chemical intuition than ELF.[50]

Recently, a one-to-one correspondence has been shown to exist between the maxima in $-\nabla^2\rho(r)$ with the maxima displayed in the conditional pair probability for same-spin electrons.[51] These latter maxima result from corresponding localizations of the Fermi density, and the correspondence demonstrates that the CCs do indeed determine the spatial regions where increased electron pairs occur, as determined by a corresponding localization of the Fermi density. The intra- and interatomic contributions to the Fermi correlation also yield to definition of localization and delocalization indices, which allow one to compare the number of localized and bonded electron pairs present in a molecule with a pairing structure predicted by the Lewis model.[42]

The theory of AIM uses the electron density, a physical property of the total system, as its starting point, regardless of how it was obtained. One example of this is the partition of experimental electron densities of a molecule into atoms in terms of the gradient vector field of $\rho(r)$ following the AIM theory. Since 1960, the distribution of the electronic density charge $\rho(r)$, as a physically observable phenomenon, has been determined experimentally by means of the diffraction of X-rays.[52a] Nevertheless, the study of molecules of medium size (20−30 atoms) with the use of conventional diffractometers and by means of a serial detection technique required periods of time as long as several weeks or even months. These difficulties meant that only qualitative results were obtained for molecules of larger size (i.e., proteins[52b]). Although, in the past few years, several developments have improved this situation substantially (synchrotron radiation at low temperature and new and better area detectors[53]), the most refined results of $\rho(r)$ required several days. These difficulties are especially true in the field of carbocations due to their short lifetime. The unstable nature of these species has prevented a detailed examination of their properties via experimental techniques. Thus, these restrictive experimental conditions demand that theoretical calculations be used to make valuable contributions. A deep knowledge of the electronic structure of these carbocationic species is essential in order to understand the mechanisms that occur during the catalytic process in the transformation of hydrocarbons.

This work is the continuation of two previous papers where the charge density topology of *n*-butoniums was studied[14] and an exploratory analysis on the usefulness and applicability of analysis of the Laplacian topology was done,[15] both at the HF/6-311++G** level of calculation. There, we investigated not only what occurs in the 3c-2e bonds but also the role of the neighboring bonds in the redistribution of the electronic charge density.

At the HF level, the only correlation is described as the Fermi correlation and corresponds to the correlation between the motions of same-spin electrons resulting from the antisymmetry requirement imposed to the wave function. The remaining correlation (the so-called Coulomb correlation) corresponds to describing specific Coulombic interactions between both opposite and same-spin electrons. This work corresponds to a study of the electronic correlation effects regarded at the MP2 (full-electron and frozen-core) level and their effects on the results obtained from the analysis previously done on carbocationic species.

Calculation Method and Analytical Details

The structures of the different species were optimized at the MP2/(full)/6-31G** level,[9b] and the systems are confirmed as true minimum in the potential energy surface by the presence of real harmonic frequencies only after one vibrational analysis. The potential energy surface of n-$C_4H_{11}^+$ cations, computed at the MP4SDTQ(fc)/6-311++G**//MP2(full)/6-31G** level and considering corrections for zero point energy and 298.15 K, showed that the most stable species is structure **11**. Structure **10** lies 0.1 kcal/mol higher in energy relative to structure **11**.[9b] The wave functions used for the topological analysis were obtained at HF and MP2 levels of calculation using the TZV and DZV schemes of contraction, adding diffuse and polarization functions for carbon and hydrogen atoms. Full-electron and frozen-core correlated calculations were done. All of these calculations were performed using the *Gaussian 98* package.[54]

The evaluation of the density and Laplacian distribution of the electronic charge densities are accomplished by means of the *AIMPAC* package.[55]

We only present here the essential theoretical information that is needed for the discussion of the numerical results, because the use of the topological concepts is well-documented in the standard literature.[16,56]

The AIM is based on the CPs of the electronic density distribution. These are points where the electronic density gradient vanishes and are characterized by the three eigenvalues (λ_1, λ_2, and λ_3) of the Hessian matrix of ρ. The CPs are labeled as (r, s) according to their rank, r (number of nonzero eigenvalues), and signature, s (the algebraic sum of the signs of the eigenvalues). A (3, −1) point, or bond critical point (BCP), is generally found between two neighboring nuclei, indicating the existence of a bond between them.

The Laplacian of ρ is defined by the equation

$$\nabla^2\rho = \partial^2\rho/\partial x^2 + \partial^2\rho/\partial y^2 + \partial^2\rho/\partial z^2$$

The relief map of the Laplacian function for the atomic system exhibits a shell of charge concentration and another one of charge depletion for each quantum shell. The outer quantum shell of an atom over $\nabla^2\rho < 0$ is called valence shell charge concentration (VSCC). For an isolated atom, a sphere is located where the valence electronic charge is maximally and uniformly concentrated. The VS loses its uniformity when the atom is within a chemical bond. The local maxima that are created provide one-to-one mapping of the electron pairs of the Lewis and VSEPR model.[16,38,39]

Topologically, the extremes or critical points in the distribution of the Laplacian function of ρ are classified by their rank and signature in the same way as is done for the CPs in the charge density. The CPs of the Laplacian appear where $\nabla(\nabla^2\rho) = 0$ and the eigenvalues of the Hessian of $\nabla^2\rho$ indicate the principal curvatures of $\nabla^2\rho$ in the CP. According to some authors,[36] it is convenient, for a more intuitive interpretation, to consider the $-\nabla^2\rho$ function. A (3, −3) CP corresponds to a local maximum in $-\nabla^2\rho$ (with $\nabla^2\rho < 0$) and indicates a local electronic CC, while a (3, +3) CP corresponds to a local minimum in $-\nabla^2\rho$ (with $\nabla^2\rho > 0$), and it indicates a local depletion of the electronic charge.

Results and Discussion

In Figure 1, we display the molecular graphs of the carbocationic species that result from the protonation of the C_2-C_3 bond in the *n*-butane molecule. They are the 2-C-*n*-butoniums labeled **10** and **11** like in our previous papers.[11] We denote the

TABLE 1: Topological Local Properties at the (3, −3) CPs of $-\nabla^2\rho(r_c)$ in the Valence Shell of the Protonates Carbon Atoms in the 2-C-*n*-Butonium Cations at the HF and Correlated MP2 (Full) Levels of Calculation[a]

HF

	10			11		
	$-\nabla^2\rho(r)$	r_c	λ_3	$-\nabla^2\rho(r)$	r_c	λ_3
			VS of C_2			
C_1	1.263	0.953	−26.871	1.264	0.953	−26.946
H	1.377	0.980	−19.468	1.364	0.981	−19.185
H	1.420	0.977	−20.122	1.417	0.978	−20.001
H*, C_3						
			VS of C_3			
H*, C_2						
H	1.416	0.978	−19.955	1.417	0.978	−20.011
H	1.408	0.978	−19.993	1.364	0.981	−19.173
C_4	1.234	0.954	−26.478	1.265	0.953	−26.963

Correlated Full Electron

	$-\nabla^2\rho(r)$	r_c	λ_3	$-\nabla^2\rho(r)$	r_c	λ_3
			VS of C_2			
C_1	1.110	0.955	−26.173	1.114	0.954	−26.327
H	1.284	0.977	−19.944	1.272	0.978	−19.705
H	1.333	0.973	−20.786	1.331	0.973	−20.722
H*						
			VS of C_3			
H*						
H	1.331	0.973	−20.706	1.331	0.973	−20.722
H	1.323	0.973	−20.682	1.272	0.978	−19.705
C_4	1.077	0.957	−25.687	1.114	0.954	−26.327

[a] Calculated using 6-311++G** basis set. r_c: distance from the (3,−3) CP to the carbon nuclei, in atomic units. All quantities are in atomic units. The symbols are explained in the text.

bond critical points (obtained from topological analysis of the electronic density) by filled circles. H* represents the incoming proton. H_0 represents the H atoms located on the protonated C (C(H*)). With H^a and $H_0{}^a$, we distinguish the C−H bonds antiperiplanar to C−H* and C−H bonds, respectively. The relevant geometrical parameters are also displayed.

In Table 1, we show the topological local properties at the (3, −3) CPs of $-\nabla^2\rho(r)$ in the VSCCs of the protonated carbon atoms in the 2-C-*n*-butonium cations at the HF and correlated MP2 (full) levels of calculation with the 6-311++G** basis set. The reported values for each carbon are the negative of the Laplacian in the (3, −3) CPs, $-\nabla^2\rho$, the distance from the CP to the carbon nuclei, r_c, and the perpendicular curvature to the surface of the sphere of charge concentration or radial curvature, λ_3.

The correlated Laplacian values at the CPs are lower compared to the HF values. The variations appear in the first decimal place. We found a decrease of ∼14% at the (3, −3) CPs on the C−C bond paths and ∼7% on the C−H paths. The differences closely follow the behavior of the correlated delocalization indices of hydrocarbons[42] (∼16% at C−C bond and ∼5% at C−H bond for C_2H_6). The r_c for the CPs in the C−H bond paths are slightly diminished by the correlation. The opposite is found for the r_c of the CPs at the C−C bond paths. Also, we found a decrease of the λ_3 values at the C−C bond paths and an increase at the C−H paths. This fact must be related to the behavior of r_c. In fact, as we have shown in previous work,[15] when the CPs are carried out toward the nuclei position, the λ_3 value grows conversely.

At both levels of calculation, no CPs at the carbon valence shells are found in the region of the 3c-2e interaction. In Figure 2a, the relief map of the $-\nabla^2\rho(r)$ distribution in compound **11** on the plane that contains the $C_2-H^*-C_3$ atoms at the MP2/6-311++G** level is shown. The nuclear CP of H* in the region of the three-centered bond can be observed, and the absence of points of charge concentration (regions where the function is locally concentrated) over the C−H* bond paths are also noted at the correlated level of calculation.

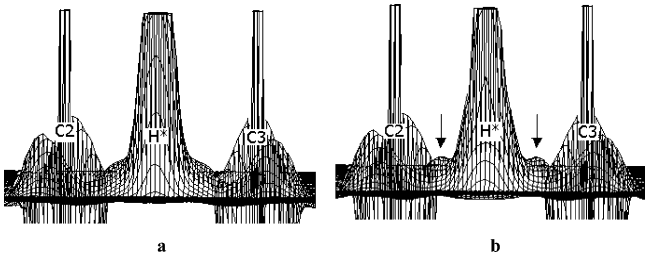

Figure 2. Relief map of the Laplacian distribution in compound **11** in the plane that contains the $C_2-H^*-C_3$ atoms at the MP2/6-311++G** level (a) and at the same level with the mixed basis set (b). The nuclear CP of H* can be observed in the region of the three center bonds. In part a, note the absence of points of charge concentration (regions where the function is locally concentrated) over the C−H* bond paths. In part b, note over the three center bonds two regions where the function is locally concentrated at the C−H* bond paths (the (3, −3) CPs indicated by arrows).

Over each classical bond path, we have always found the corresponding Laplacian CCs. Nevertheless, the VSCCs at the 3c-2e bond paths do not appear at correlated or uncorrelated calculations. In previous work, we found that basis sets with diffuse functions could introduce difficulties into the definition of some Laplacian (3, −3) CPs.[57] So, to study the effect of some basis sets over the topology of the Laplacian function at the 3c-2e region, we analyzed the systems with several basis sets (among them a 6-311 scheme, the same scheme with polarization functions, the same scheme with only diffuse functions, and the same combinations with a 6-31 scheme).[57] We have found that it is only necessary to replace the TZV scheme for the DZV at the H* atom to make possible the definition of the subtle VSCC (3, −3) PCs at C(H*)−H*.

In Table 2 are shown the topological local properties at the (3, −3) CPs of $-\nabla^2\rho(r_c)$ in the valence shell of the protonated carbon atoms in the 2-C-*n*-butonium cations at the HF and correlated MP2 (full and frozen-core) levels of calculation using a mixed basis set. The mixed basis set scheme consists of using a 6-31 basis set with polarization and diffuse functions for H* and a 6-311++G** basis set for all other atoms. This particular scheme allows us to detect the subtle 3c-2e VS PCs, keeping the definition of almost all atoms the same as in previous calculations. This is important in order to maintain the description of the neighboring interactions unaltered. Also, in Table 2, the VSCCs of adjacent carbon atoms are studied. The ellipticity, defined by the relationship between the two tangential curvatures, λ_1 and λ_2, $\epsilon = (\lambda_1/\lambda_2) - 1$, is also reported. The most notable characteristics are the presence of a subtle (3, −3) CP at the valence shell of the protonated carbons in the region of the 3c-2e interaction, both at correlated and uncorrelated levels of calculation. These CPs have $-\nabla^2\rho(r_c)$ and λ_3 values lower by 1 order of magnitude than the typical VS (3, −3) CPs and are the farthest from the C(H*) nuclei position. In Figure 2b, we show the relief map of the Laplacian distribution in compound **11** in the plane that contains the $C_2-H^*-C_3$ atoms at the MP2 level with the mixed basis set. We observe the nuclear CP of H* and, over the three-centered bond, two regions where the function is locally concentrated (the (3, −3) CPs indicated by arrows in Figure 2b) at the C−H* bond paths. Because the Laplacian CCs are related to regions where

TABLE 2: Topological Local Properties at the (3, −3) CPs of $-\nabla^2\rho(r_c)$ in the Valence Shell of the Protonates' Carbon Atoms in the 2-C-*n*-Butonium Cations (Structures 10 and 11) at the HF and Correlated MP2 (Full and Frozen-Core) Levels of Calculation Using the Mixed Basis Set[a]

HF

	10				11			
	$-\nabla^2\rho(r)$	r_c	λ_3	ϵ	$-\nabla^2\rho(r)$	r_c	λ_3	ϵ
				VS of C_1				
H[a]	1.167	1.014	−13.890	0.0216	1.169	1.014	−13.903	0.0225
H	1.217	1.010	−14.582	0.0414	1.219	1.010	−14.637	0.0417
H	1.207	1.012	−14.298	0.0414	1.207	1.012	−14.295	0.0415
C_2	0.845	1.044	−10.387	0.0684	0.843	1.044	−10.301	0.0676
				VS of C_2				
C_1	1.264	0.953	−26.937	0.0752	1.265	0.952	−27.017	0.0742
H_0[a]	1.381	0.980	−19.575	0.0797	1.369	0.981	−19.280	0.0786
H_0	1.420	0.977	−20.163	0.0797	1.417	0.978	−20.043	0.0798
H*, C_3	0.259	1.210	−2.096	0.6224	0.269	1.202	−2.164	0.4028
				VS of C_3				
H*, C_2	0.273	1.203	−2.114	0.6798	0.268	1.202	−2.162	0.3978
H_0	1.416	0.978	−20.010	0.0790	1.417	0.977	−20.053	0.0798
H_0[a]	1.410	0.977	−20.092	0.0803	1.368	0.981	−19.266	0.0785
C_4	1.238	0.954	−26.587	0.0714	1.266	0.952	−27.032	0.0742
				VS of C_4				
C_3	0.820	1.046	−10.203	0.0718	0.843	1.044	−10.303	0.0678
H	1.216	1.010	−14.565	0.0413	1.208	1.012	−14.300	0.0417
H	1.226	1.009	−14.809	0.0397	1.219	1.010	−14.626	0.0417
H[a]	1.165	1.014	−13.854	0.0203	1.168	1.014	−13.901	0.0226

MP2 (Full)

	$-\nabla^2\rho(r)$	r_c	λ_3	ϵ	$-\nabla^2\rho(r)$	r_c	λ_3	ϵ
				VS of C_1				
H[a]	1.091	1.008	−14.731	0.0183	1.093	1.008	−14.740	0.0198
H	1.148	1.003	−15.583	0.0403	1.151	1.002	−15.644	0.0405
H	1.140	1.004	−15.372	0.0402	1.140	1.004	−15.375	0.0405
C_2	0.757	1.031	−12.034	0.0909	0.755	1.031	−11.935	0.0891
				VS of C_2				
C_1	1.111	0.954	−26.236	0.0480	1.115	0.954	−26.383	0.0500
H_0[a]	1.288	0.976	−20.034	0.0691	1.277	0.978	−19.779	0.0684
H_0	1.333	0.973	−20.832	0.0744	1.331	0.973	−20.766	0.0759
H*, C_3	0.287	1.125	−4.377	0.1101	0.292	1.123	−4.453	0.1770
				VS of C_3				
H*, C_2	0.301	1.120	−4.662	0.1924	0.291	1.123	−4.443	0.1875
H_0	1.332	0.973	−20.759	0.0748	1.331	0.973	−20.772	0.0759
H_0[a]	1.324	0.973	−20.771	0.0740	1.276	0.978	−19.758	0.0682
C_4	1.081	0.957	−25.772	0.0404	1.116	0.954	−26.398	0.0502
				VS of C_4				
C_3	0.732	1.033	−11.806	0.0994	0.756	1.031	−11.939	0.0890
H	1.149	1.002	−15.642	0.0406	1.140	1.004	−15.379	0.0405
H	1.160	1.001	−15.875	0.0380	1.150	1.002	−15.630	0.0407
H[a]	1.090	1.007	−14.738	0.0166	1.093	1.008	−14.736	0.0200

FC

	$-\nabla^2\rho(r)$	r_c	λ_3	ϵ	$-\nabla^2\rho(r)$	r_c	λ_3	ϵ
				VS of C_1				
H[a]	1.093	1.007	−14.786	0.0183	1.095	1.007	−14.795	0.0198
H	1.150	1.002	−15.641	0.0402	1.153	1.002	−15.702	0.0403
H	1.142	1.003	−15.430	0.0400	1.142	1.003	−15.432	0.0405
C_2	0.760	1.030	−12.110	0.0907	0.757	1.031	−12.010	0.0889
				VS of C_2				
C_1	1.114	0.954	−26.332	0.0479	1.118	0.954	−26.480	0.0499
H_0[a]	1.290	0.976	−20.093	0.0690	1.279	0.977	−19.838	0.0684
H_0	1.335	0.972	−20.892	0.0744	1.333	0.973	−20.825	0.0760
H*, C_3	0.287	1.124	−4.417	0.1107	0.293	1.122	−4.493	0.1770
				VS of C_3				
H*, C_2	0.302	1.119	−4.704	0.1924	0.292	1.122	−4.483	0.1882
H_0	1.333	0.973	−20.819	0.0747	1.333	0.973	−20.831	0.0759
H_0[a]	1.326	0.973	−20.831	0.0739	1.278	0.977	−19.816	0.0680
C_4	1.084	0.956	−25.868	0.0403	1.119	0.953	−26.495	0.0501
				VS of C_4				
C_3	0.734	1.032	−11.881	0.0991	0.758	1.031	−12.015	0.0891
H	1.151	1.002	−15.700	0.0404	1.142	1.003	−15.436	0.0405
H	1.161	1.000	−15.933	0.0379	1.152	1.002	−15.689	0.0405
H[a]	1.091	1.007	−14.794	0.0164	1.095	1.007	−14.791	0.0198

[a] r_c is the distance from the (3, −3) CP to the carbon nuclei, in atomic units. All quantities are in atomic units. ϵ is dimensionless. The symbols are explained in the text.

TABLE 3: Differences of the Values of the Topological Properties at Each (3, −3) CP in the 2-C-Butonium 10 and 11 with Respect to the Corresponding Values of the *n*-Butane Molecule at the HF and Correlated MP2 (Frozen-Core) Levels of Calculation Using the Mixed Basis Set[a]

	HF								MP2							
	10				**11**				**10**				**11**			
	$-\nabla^2\rho(r)$	r_c	λ_3	ϵ	$-\nabla^2\rho(r)$	r_c	λ_3	ϵ	$-\nabla^2\rho(r)$	r_c	λ_3	ϵ	$-\nabla^2\rho(r)$	r_c	λ_3	ϵ
							VS of C_1									
H[a]	0.029	−0.011	−1.420	0.0120	0.031	−0.011	−1.433	0.0129	0.014	−0.007	−0.9923	0.0097	0.0158	−0.0072	−1.0013	0.0112
H	0.085	−0.016	−2.288	0.0326	0.087	−0.016	−2.343	0.0329	0.075	−0.013	−1.9739	0.0313	0.0782	−0.0131	−2.0349	0.0314
H	0.075	−0.014	−2.004	0.0326	0.075	−0.014	−2.001	0.0327	0.067	−0.012	−1.7631	0.0311	0.0672	−0.0121	−1.7651	0.0316
C_2	−0.126	0.046	7.003	0.0617	−0.128	0.046	7.089	0.0609	−0.103	0.036	5.8863	0.0862	−0.1062	0.0374	5.9863	0.0844
							VS of C_2									
C_1	0.302	−0.047	−9.934	0.0662	0.303	−0.048	−10.014	0.0652	0.234	−0.036	−7.809	0.0282	0.238	−0.036	−7.957	0.0302
H_0[a]	0.243	−0.045	−7.250	0.0696	0.231	−0.044	−6.955	0.0685	0.208	−0.037	−6.194	0.0593	0.197	−0.036	−5.939	0.0587
H_0	0.282	−0.048	−7.837	0.0688	0.279	−0.047	−7.717	0.0689	0.253	−0.041	−6.993	0.0647	0.251	−0.04	−6.926	0.0663
							VS of C_3									
H_0	0.278	−0.047	−7.684	0.0687	0.279	−0.048	−7.727	0.0695	0.251	−0.040	−6.92	0.0650	0.251	−0.04	−6.932	0.0662
H_0[a]	0.272	−0.048	−7.766	0.0702	0.230	−0.044	−6.940	0.0684	0.244	−0.040	−6.932	0.0642	0.196	−0.036	−5.917	0.0583
C_4	0.276	−0.045	−9.584	0.0626	0.304	−0.047	−10.029	0.0654	0.204	−0.034	−7.345	0.0206	0.239	−0.037	−7.972	0.0304
							VS of C_4									
C_3	−0.151	0.048	7.186	0.0651	−0.128	0.046	7.086	0.0611	−0.129	0.0384	6.1153	0.0946	−0.1052	0.0374	5.9813	0.0846
H	0.084	−0.016	−2.272	0.0325	0.076	−0.014	−2.007	0.0329	0.076	−0.0131	−2.0331	0.0315	0.0672	−0.0121	−1.7691	0.0316
H	0.094	−0.017	−2.516	0.0309	0.087	−0.016	−2.333	0.0329	0.086	−0.0151	−2.2659	0.0290	0.0772	−0.0131	−2.0219	0.0316
H[a]	0.027	−0.011	−1.384	0.0107	0.030	−0.011	−1.431	0.0130	0.012	−0.0072	−1.0003	0.0078	0.0158	−0.0072	−0.9973	0.0112

[a] A positive value means an increment of the parameter in the protonated species, and a negative value means that the parameter in the C-*n*-butonium is lower compared to that in the *n*-butane. r_c: distance from the (3, −3) CP to the carbon nuclei. All quantities are in atomic units. ϵ is dimensionless. The symbols are explained in the text.

increased electron pairing occurs, these kinds of subtle critical points should be typical from interactions deficient in electrons such as the 3c-2e ones, because there is only one electron pair for three atomic centers in them.

At the VSCCs of the C(H*) atoms, the correlated CPs at the 3c-2e bond path are closer to the C(H*) nuclei, and their values of $-\nabla^2\rho(r_c)$ and λ_3 are larger than the uncorrelated ones. The opposite trend is found for the ellipticity values: The correlated ϵ value diminishes. At all other VSCCs of C(H*) atoms, the behavior of the correlated topological properties with respect to the noncorrelated ones is similar to that found with the previous basis set (see Table 1). The r_c for the CPs in the C−C bond path is slightly augmented by the correlation. The opposite is found for the r_c of the CPs at the C−H bond paths. The correlated ellipticity values at the CPs are lower than the HF ones. We found a decrease of ∼56% at the (3, −3) CPs on the C−C bond paths and between ∼7% and ∼15% on the C−H ones, which shows (now, over another topological property) a larger Coulomb correlation effect over C−C bonds than over C−H ones. The variations on correlated ϵ's on C−H bonds are interestingly related to the spatial disposition of the bonds. The greater correlation effect is found in the bonds that are antiperiplanar with respect to a C−H bond (∼15% on the C−H[a] bond paths and ∼7% on the C−H paths). This effect consists of correcting the overestimation produced at the HF level over ϵ. The negative curvatures of λ_2 and λ_3 that define ϵ are perpendicular to the CP nuclei vector at the (3, −3) CP; therefore, a spherical VSCC CP would have ϵ equal to zero. Thus, the ϵ values can be related to electronic delocalization concepts: A larger difference with respect to a spherical shape (larger ϵ value) means larger differential delocalization.[30] Our work shows that the effect of the electronic correlation over the differential electronic delocalization is larger over C−H bonds that are antiperiplanar to another C−H bond.

The Laplacian at the CPs of the adjacent carbon atoms follow the same behavior as the VSCC CPs of C(H*), although the variations are slighter. Moreover, all correlated r_c values are lower than the uncorrelated; therefore, all correlated λ_3 values are higher than the uncorrelated ones. This fact can be rationalized as an attraction of the VS toward the nuclei.

The correlated ellipticity on the C−C CP, unlike on the other CPs, increases by 24%, showing an HF underestimation over this parameter. At the C−H bond path, we found, the same as the C(H*) VS, a decrease in correlated ϵ and a greater correlation effect in the bonds that are antiperiplanar with respect to the C−H* bond (∼18% at the (3, −3) CPs on the C−H[a] bond paths and ∼3% on the C−H paths). Also, at the VS of the adjacent carbon atoms, we found a larger Coulomb correlation effect over C−C bond paths than over C−H ones.

The frozen-core correlated calculation shows small differences with respect to the full calculation (see Table 2). The trends observed are totally similar to those obtained within a full-electron scheme. However, within frozen-core calculations, we found Laplacian values slightly higher and r_c's and λ_3's slightly shorter than the full-electron ones. The ellipticity values are approximately the same. Then, the correlation effect introduced by the core electrons increases the r_c values and consequently diminishes the λ_3 and Laplacian values. These facts show the sensitivity of Laplacian PCs to an "intershell" electronic repulsion effect between the valence shell and core electrons, clearly showing the shielding effect of the core density to the nuclear attraction. Nevertheless, owing to the shortness in the variations found, further analysis of the Laplacian topology will be done at MP2 frozen-core level.

In Table 3, we show the differences (Δ's) of the values of topological properties for each CP in the 2-C-butonium structures **10** and **11** with respect to the corresponding values in the *n*-butane molecule. We show the HF and MP2(fc) values using the already defined mixed basis set scheme. The values reported can be used to study the perturbation introduced in the system by the incoming proton. A positive value means an increment of the parameter in the protonated species, and a negative value means that the parameter in the C-*n*-butonium is lower than in *n*-butane. The (3, −3) correlated CPs corresponding to the VS of the C(H*) are displaced toward the nuclei, and the values of

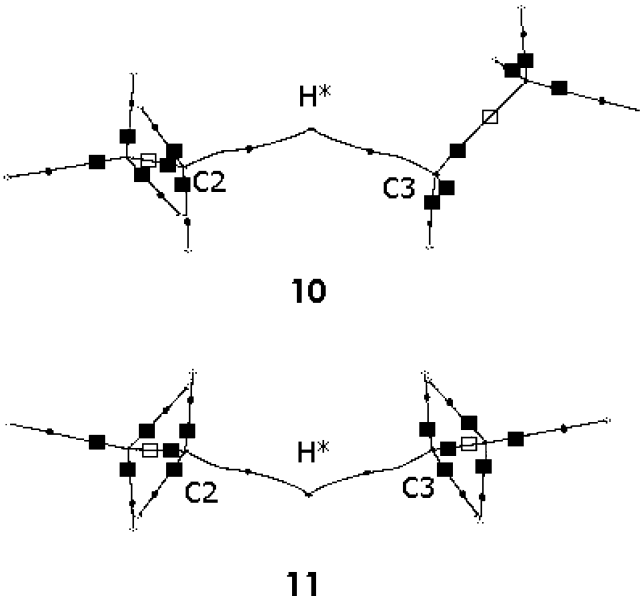

Figure 3. Molecular graphs of the species **10** and **11** where the location of VS (3, −3) CPs of the Laplacian of the electronic density are indicated approximately on the VS of each carbon atom. With empty (filled) squares are indicated the CPs that go away from (come closer to) the carbon atom. The bond critical points (obtained from topological analysis of the electronic density) are denoted by filled circles.

the Laplacian, the perpendicular curvature, and the ellipticity are augmented. Similar changes, although of lower magnitude, are observed on the VS of the adjacent carbon atoms, in the C−H bond paths. Besides, an asymmetrical distribution is clearly observed on the C−C bonds, depending on CP spatial localization in relation to the protonation site. The shifting of the VSCC CPs toward the electron-deficient region at the 3c-2e bonds is represented graphically in Figure 3, where displacements experienced by each VSCC CP in structures **10** and **11** with respect to *n*-butane are shown. All these features are totally similar to those found at an uncorrelated level reported in our previous work,[15] where the 1-C-*n*-butonium (three overall), the 1-H-*n*-butonium (three overall), and the 2-H-*n*-butonium (three overall) species where also anlyzed. Although correlated $\Delta(-\nabla^2\rho(r))$, Δr_c, and $\Delta\lambda_3$ values are less than uncorrelated[15] ones, the results indicate clearly that the electronic density delocalizes through the σ-bonds at C−C and C−H of the molecule toward the protonation site, which has the highest requirements of electronic density.

The variations on the correlated ellipticity ($\Delta\epsilon$), as in the other parameters, are lower than the uncorrelated ones. This fact indicates a slight HF overvaluation on the effect of the incoming proton. The exception is the CP over the C−C bond path in the VSCCs of the adjacent carbon atoms, where the correlated variation is augmented by ∼28%. This feature must be related to the behavior of the VS CP of C(H*) at the same C−C bond path, and therefore, it could also be one effect of the electronic deficiency of C(H*), which appears confined within the C−C bond path.

Analyzing correlated $\Delta\epsilon$ (comparison between the protonated structure and butane at the same level of calculation) with respect to uncorrelated $\Delta\epsilon$, the greater differences are on the C−C bonds: Near C(H*), we found decreasing $\Delta\epsilon$, and near adjacent C, we found increasing $\Delta\epsilon$. Moreover, over the C−H bonds, the greater correlation effects on $\Delta\epsilon$ are at C−H^a or C−H$_0^a$ bonds. These trends are similar to those encountered when we analyzed the behavior of correlated ϵ (comparison between both levels of calculation at the same structure).

TABLE 4: Topological Local Properties of the Charge Density at the Bonding CPs of 2-C-*n*-Butonium for the C(H*)−C and C(H*)−H* Bonds at HF and Correlated MP2 (Full-Electron) Levels of Calculation Using the Mixed Basis Set

bond		ρ_{cp}	$\nabla^2\rho_{cp}$	ϵ	T	V	K
			10				
C_1-C_2	MP2	0.254	−0.635	0.018	0.076	−0.311	0.235
		(0.255)[a]	*(−0.636)*	*(0.018)*	*(0.076)*	*(−0.311)*	*(0.235)*
	HF	0.264	−0.767	0.015	0.071	−0.334	0.263
C_2-H^*	MP2	0.165	−0.257	0.085	0.0670	−0.198	0.131
		(0.164)	*(−0.257)*	*(0.081)*	*(0.067)*	*(−0.198)*	*(0.131)*
	HF	0.161	−0.256	0.109	0.077	−0.220	0.142
H^*-C_3	MP2	0.167	−0.272	0.071	0.067	−0.202	0.135
	HF	0.163	−0.272	0.090	0.078	−0.225	0.146
C_3-C_4	MP2	0.249	−0.608	0.025	0.075	−0.303	0.227
	HF	0.259	−0.740	0.019	0.070	−0.326	0.255
			11				
C_1-C_2	MP2	0.253	−0.635	0.018	0.076	−0.311	0.235
	HF	0.264	−0.766	0.015	0.071	−0.335	0.263
C_2-H^*	MP2	0.166	−0.261	0.116	0.067	−0.201	0.133
	HF	0.163	−0.265	0.140	0.078	−0.222	0.144
H^*-C_3	MP2	0.166	−0.260	0.122	0.067	−0.200	0.132
	HF	0.163	−0.264	0.146	0.077	−0.222	0.144
C_3-C_4	MP2	0.254	−0.635	0.018	0.076	−0.311	0.235
	HF	0.264	−0.767	0.015	0.071	−0.335	0.263

[a] In italics are the MP2 frozen-core values.

TABLE 5: Topological Local Properties of the Charge Density at the Bonding CPs of 2-C-*n*-Butonium for the C−H$_0$ Bonds at HF and Correlated MP2 (Full-Electron) Levels of Calculation Using the Mixed Basis Set

		ρ_{cp}	$\nabla^2\rho_{cp}$	ϵ	T	V	K
			10				
$C_2-H_0^a$	MP2	0.283	−1.013	0.022	0.037	−0.329	0.291
		(0.283)[a]	*(−1.014)*	*(0.022)*	*(0.037)*	*(−0.329)*	*(0.291)*
	HF	0.293	−1.108	0.029	0.028	−0.334	0.306
C_2-H_0	MP2	0.289	−1.049	0.028	0.037	−0.337	0.299
		(0.289)	*(−1.050)*	*(0.028)*	*(0.037)*	*(−0.337)*	*(0.299)*
	HF	0.298	−1.144	0.034	0.028	−0.342	0.314
			11				
$C_2-H_0^a$	MP2	0.282	−1.005	0.021	0.038	−0.328	0.289
	HF	0.292	−1.101	0.028	0.029	−0.333	0.304
C_2-H_0	MP2	0.289	−1.050	0.029	0.037	−0.337	0.300
	HF	0.298	−1.144	0.034	0.028	−0.343	0.314

[a] In italics are the MP2 frozen-core values.

TABLE 6: Topological Local Properties of the Charge Density at the Bonding CPs of 2-C-*n*-Butonium for the C−H$_3$ Bonds at HF and Correlated MP2 (Full-Electron) Levels of Calculation Using the Mixed Basis Set

		ρ_{cp}	$\nabla^2\rho_{cp}$	ϵ	T	V	K
			10				
C_1-H	MP2	0.280	−0.964	0.017	0.045	−0.331	0.286
		(0.280)[a]	*(−0.965)*	*(0.017)*	*(0.045)*	*(−0.331)*	
	HF	0.287	−1.049	0.019	0.037	−0.338	0.300
C_1-H^a	MP2	0.272	−0.917	0.007	0.045	−0.319	0.274
		(0.272)	*(−0.918)*	*(0.007)*	*(0.045)*	*(−0.320)*	
	HF	0.280	−1.004	0.009	0.038	−0.327	0.289
C_1-H	MP2	0.279	−0.959	0.017	0.045	−0.330	0.285
		(0.279)	*(−0.960)*	*(0.017)*	*(0.045)*	*(−0.331)*	
	HF	0.286	−1.044	0.020	0.038	−0.338	0.299
			11				
C_1-H	MP2	0.280	−0.965	0.017	0.045	−0.331	0.286
	HF	0.287	−1.050	0.019	0.037	−0.338	0.300
C_1-H^a	MP2	0.272	−0.919	0.007	0.045	−0.320	0.275
	HF	0.280	−1.006	0.010	0.038	−0.327	0.289
C_1-H	MP2	0.280	−0.959	0.017	0.045	−0.331	0.285
	HF	0.286	−1.044	0.020	0.038	−0.338	0.299

[a] In italics are the MP2 frozen-core values.

We report in Tables 4, 5, and 6 the topological local properties of the electronic charge density, $\rho(r)$, at the BCPs of the

2-C-*n*-butonium for the C(H*)−C and C(H*)−H* bonds, C(H*)−H_0 bonds, and C−H_3 bonds, respectively, at HF and correlated MP2 (full-electron) levels of calculation using the mixed basis set previously defined. The values of charge density (ρ_b), Laplacian ($\nabla^2\rho_b$), ellipticity, ϵ, and kinetic, potential, and total electronic energy densities (T_b, V_b, and E_{eb}, respectively) at the BCPs are displayed. The topological properties at both correlated and uncorrelated BCPs on the C−C bonds (see Table 4) show the same differences from the typical C−C bond of normal hydrocarbons.[14] The correlated results also indicate that the C−H* and C−H_0 bonds (see Tables 4 and 5) can be characterized as covalent bonds or shared interactions. They show significant differences: ρ_b and $\nabla^2\rho_b$ values at the C−H* bonds are lower than those at the C−H_0 bond paths, indicating a weakened interaction. The ellipticities of these bonds are significantly higher than the values found for the other C−H_0 (see Table 5) or C−H bonds (see Table 6). These observations are in agreement with a delocalization of electron charge density. The values of kinetic density, T_b, and potential energy density, V_b, at the C−H* bond paths are greater and lower, respectively, than the same properties at C−H_0 (see Table 5) or another C−H (see Table 6) taken as reference. These facts clearly show the distinctive characteristic topological properties of the interaction at the 3c-2e bond, C−H*−C. The results are in accordance with previous results realized at HF level[14] and demonstrate that the main topological features of ρ_b at the 3c-2e interaction are equally depicted at both correlated and uncorrelated levels of calculation.

The correlated values of the topological parameters of the electronic charge density distribution (ρ_b and $\nabla^2\rho_b$), like in the topology of the Laplacian distribution, are lower than the uncorrelated one.

The variations in ρ_b and $\nabla^2\rho_b$ are ∼4% and ∼20%, respectively, for C(H*)−C bonds (Table 4), ∼3% and ∼9%, respectively, for C−H_0 and C−H_3 bonds (Tables 5, 6), and ∼2% and 0.2%, respectively, for C−H* bonds (Table 4). In 2c-2e interactions (classical bonds), the correlation effects are higher in $\nabla^2\rho_b$ than in ρ_b. The largest correlation effect is over $\nabla^2\rho_b$ at the C−C bond path. At the 3c-2e bond paths, the correlation effects in ρ_b are higher than in $\nabla^2\rho_b$.

The ellipticity on a BCP (ϵ_{bcp}), like ϵ on a VSCC PC, is directly related to the curvatures of the function whose topology is analyzed. Within $\rho(r)$ topology, ϵ indicates the deviation of the electronic charge density from axial symmetry of a chemical bond providing a quantitative measure of the π-character of the bond or the delocalization of electronic charge. Our results reflect an HF overestimation for ϵ_{bcp} at C−H bonds. The correlated ϵ_{bcp} is lower than the uncorrelated value in any C−H BCP, and there, the correlated kinetic energy grows. Instead, at C−C bonds, we found that the Coulomb correlation increases the ϵ_{bcp} value, showing the HF subvaluation of ϵ_{bcp}. The correlated ϵ at the C−C BCP is larger than the uncorrelated value, and both the correlated kinetic and correlated potential energies diminish. The Coulombic effect is greatest in C−$H_0{}^a$ and C−H^a bond paths (29% and 32%, respectively). The variations found in ρ_b and $\nabla^2\rho_b$ values are ∼3% and ∼9%, respectively. Our results indicate that, like in $\nabla^2\rho$ topology, ϵ_{bcp} is the parameter most affected by the correlation effects.

In Table 7, we present the analysis of the topological properties of local properties at the nuclear (3, −3) CPs of $-\nabla^2\rho(r_c)$ of hydrogen atoms in structure **10** at the HF and correlated MP2 (frozen-core) levels of calculation using the mixed basis set. It is worth noting the negligible effect of the electronic correlation in the mentioned parameters (∼0.50%). Nevertheless, over the H* parameters, the correlation effect is ∼4%.

TABLE 7: Topological Local Properties at the Nuclear (3, −3) CPs of $-\nabla^2\rho(r_c)$ of Hydrogen Atoms in Structure 10 at the HF and Correlated MP2 (Frozen-Core) Levels of Calculation Using the Mixed Basis Set[a]

	HF		MP2	
	$-\nabla^2\rho(r)$	$\rho(r)$	$-\nabla^2\rho(r)$	$\rho(r)$
C_1−H_3				
H^a	24.647	0.415	24.759	0.412
H	25.225	0.425	25.400	0.422
H	25.256	0.426	25.410	0.422
C_2−H_2				
$H_0{}^a$	24.771	0.418	24.952	0.415
H_0	25.218	0.425	25.427	0.422
H*	20.865	0.447	19.913	0.424
C_3−H_2				
H*	20.706		19.799	
H_0	25.280	0.426	25.490	0.423
$H_0{}^a$	25.124	0.423	25.332	0.420
C_4−H_3				
H	25.241	0.425	25.414	0.422
H	25.225	0.425	25.385	0.422
H^a	24.640	0.415	24.719	0.410

[a] r_c: distance from the (3, −3) CP to the carbon nuclei, in atomic units. All quantities are in atomic units. The symbols are explained in the text.

On the other hand, it is very interesting to again note the capability of the topological analysis of $-\nabla^2\rho(r)$ to discriminate among the H atoms depending on their spatial localization. By analyzing the nuclear CPs, it is easily seen that the smaller values of the Laplacian are over H^a or $H_0{}^a$ atoms. This means that over those nuclei are the lower charge concentrations, which can be interpreted as lower electronic overlapping. The C−H^a bonds are antiperiplanar to bonds deficient in electrons (C−H*), and therefore, this fact must be in line with the hyperconjugative interactions in which they are involved.

Concluding Remarks

In this work, it is shown that in protonated and neutral compounds the correlated $-\nabla^2\rho(r)$ values at the VS CCs are lower than the HF ones. Because of the relationship between those CCs and the spatial regions where increased electron pairing occurs, this fact reflects decreasing electron pairing in bonding regions according to the effect of Coulomb correlation, which disrupts the distribution of electron pairs between atoms, thus reducing the number of shared electrons. Our results also indicate the Coulomb correlation causes the increase of attraction of the nucleus for the density within its own basin. This outcome is in concordance with the results of the analysis of correlated and uncorrelated localization and delocalization indices.[42]

On the other hand, the correlation effect at the $-\nabla^2\rho(r)$ value is larger over C−C bonds than over C−H bonds. The differences found closely follow the behavior of the correlated delocalization indices of hydrocarbons[42] and also allow us to show that the Coulomb correlation effect over CCs and delocalization indices are indeed very similar, emphasizing the fact that both properties describe the electron pairing.

Our values indicate the Hartree−Fock overestimation of the electronic perturbation produced by the incoming proton.

We demonstrate that the effect of the electronic correlation over the differential electronic delocalization appears larger over C−H bonds that are antiperiplanar to the C−C (or another C−H) bond. This fact allows us to establish the Hartree−Fock

overvaluation of the differential delocalization in hyperconjugative interactions. These results show the applicability of this kind of analysis to the study of some chemical effects, and on the other hand, they suggest the necessity to use correlated wave functions for the topological study of them. Moreover, the greatest correlation effect found over ellipticities of CPs arising from both studied fields is the following: $-\nabla^2\rho(r)$ and $\rho(r)$ reveal that the correlated wave functions are appropriate for the study of aspects related to differential electronic delocalization on the σ-bonds.

Our work also shows the sensitivity of Laplacian CCs to the electronic repulsion effect against valence shell and core electrons, showing how the core electronic distribution shields the attractive effect of the nuclei for the electron valence density.

Besides, the topological description of the Laplacian for electron-deficient bonds appears highly sensitive to the basis set composition both at correlated as well as at uncorrelated levels of calculation.

The correlated topological local properties of the charge density, ρ_b and $\nabla^2\rho_b$, as in the topology of the Laplacian of $\rho(r)$, are lower than the uncorrelated properties. This is in agreement with the well-documented Hartree−Fock density overestimation of the amount of density accumulated in the internuclear region.[24] The Coulomb correlation has a larger effect at C−C bonds than at C−H bonds, and it is highly sensitive to their spatial localization, features also found in the Laplacian topology.

It is worth stressing that this theoretical study, where no orbital model is assumed, is based on a real physical property of the system. It has been performed on species in which the experimental determinations of charge density are practically impossible, strongly reinforcing the importance of this kind of analysis that allows us to conclude the following: The role of the neighboring bonds of the 3c-2e interaction, in the redistribution of the electronic charge density, can be seen in the topology of Laplacian distribution through the shifting of the critical points of concentration charge toward the electron-deficient region at the 3c-2e bonds, both through correlated as well as uncorrelated wave functions. Moreover, our results arising from the study of correlated $\rho(r)$ topology are in agreement with the previous Hartree−Fock results.[14] We also demonstrate that the main topological features of $\rho(r)$ at the 3c-2e interaction and on all other bond paths are equally depicted at both correlated and uncorrelated levels of calculation. Therefore, once reliable (correlated) carbocationic structures are found and despite the really notable effects that Coulomb correlation has over $\rho(r)$ and $\nabla^2\rho(r)$, the main features of the electronic distribution in electron-deficient systems still seem not to be sensitive to the inclusion of these correlations. In other words, our work allows us to show that the Fermi correlation, taken into account at both levels of calculation, is the main correlation responsible for the effects that explain, through topological analysis of Laplacian distribution, the MP2/(full) 6-31G** stability order of the C-*n*-butonium species: 2-C-*n*-butonium > 1-C-*n*-butonium > 2-H-*n*-butonium > 1-H-*n*-butonium.

Acknowledgment. The authors N.M.P., G.L.S., and R.M.L. thank the SECYT UNNE for financial support. A.H.J. is member of the Scientist Research career of CICPBA, Argentina. N.M.P. is a member of the Research Carrier of CONICET, Argentina.

References and Notes

(1) Field, F. H.; Munson, M. S. B. *J. Am. Chem. Soc.* **1965**, *87*, 3289.
(2) Hiraoka, K.; Kebarle, P. *J. Am. Chem. Soc.* **1976**, *98*, 6119−6125.
(3) (a) Boo, D. W.; Lee, Y. T. *Chem. Phys. Lett.* **1993**, *211*, 358. (b) Boo, D. W.; Lee, Y. T. *J. Chem. Phys.* **1995**, *103*, 520. (c) Boo, D. W.; Liu, Z. F.; Suits, A. G.; Lee, Y. T. *Science* **1995**, *269*, 57. (d) Bunker, P. R. *J. Mol. Spectrosc.* **1996**, *176*, 297. (e) Boo, P. W.; Loe, Y. T. *Int. J. Mass Spectrom. Ion Processes* **1996**, *159*, 209.
(4) (a) Yeh, L. I.; Price, J. M.; Lee, Y. T. *J. Am. Chem. Soc.* **1989**, *111*, 5597. (b) Obata, S.; Hirao, K. *Bull. Chem. Soc. Jpn.* **1993**, *66*, 3271.
(5) Carneiro, J. W. M.; Schleyer, P. v. R.; Saunders, M.; Remington, R.; Schaefer, H. F., III.; Rauk, A.; Sorensen, T. S. *J. Am. Chem. Soc.* **1994**, *116*, 3483−3493.
(6) East, A. L. L.: Liu, Z. F.; McCague, C.; Cheng, K.; Tse, J. S. *J. Phys. Chem. A* **1998**, *108*, 10903
(7) Esteves, P. M.; Mota, C. J. A.; Ramirez-Solis, A.; Hernandez-Lamoneda, R. *J. Am. Chem. Soc.* **1998**, *120*, 3213.
(8) Mota, C. J. A.; Esteves, P. M.; Ramírez-Solís, A.; Hernández-Lamoneda, R. *J. Am. Chem. Soc.* **1997**, *119*, 5193−5199.
(9) (a) Esteves, P. M.; Mota, C. J. A.; Ramírez-Solís; Hernández-Lamoneda, R. *Top. Catal.* **1998**, *6(1−4)*, 163−168. (b) Esteves, P. M.; Alberto, G. G. P.; Ramirez-Solís, A.; Mota, C. J. A. *J. Phys. Chem. A* **2000**, *104*, 6233.
(10) (a) Collins, S. J.; O'Malley, P. J. *Top. Catal.* **1998**, *6*, 151−161. (b) Collins, S. J.; O'Malley, P. J. *Chem. Phys. Lett.* **1994**, *228*, 246. (c) Collins, S. J.; O'Malley, P. J. *J. Chem. Soc., Faraday Trans.* **1996**, *92*, 4347.
(11) Esteves, P. M.; Alberto, G. G. P.; Ramírez-Solís, A.; Mota, C. J. A. *J. Am. Chem. Soc.* **1999**, *121*, 7345−7348.
(12) (a) Olah, G. A.; Halpern, Y.; Shen, J.; Mo, Y. K. *J. Am. Chem. Soc.* **1973**, *95*, 4960−4970. (b) Olah, G. A. *Angew. Chem., Int. Ed. Engl.* **1973**, *12*, 173. (c) Olah, G. A.; Prakash, G. K. S.; Williams, R. E.; Field, L. D.; Wade, K. *Hypercarbon Chemistry*; Wiley: New York, 1987.
(13) (a) Okulik, N.; Peruchena, N. M..; Esteves, P. M.; Mota, C.; Jubert, A. H. *J. Phys. Chem. A* **1999**, *103*, 8491. (b) Okulik, N.; Peruchena, N. M.; Esteves, P. M.; Mota, C.; Jubert, A. H. *J. Phys. Chem. A* **2000**, *104*, 7586.
(14) Okulik, N.; Esteves, P. M.; Mota, C.; Jubert, A. H.; Peruchena, N. M. *J. Phys. Chem. A* **2002**, *106*, 1584−1595.
(15) Lobayan, R. M.; Sosa, G. L.; Jubert, A. H.; Peruchena, N. M *J. Phys. Chem. A* **2004**.
(16) Bader, R. F. W. *Atoms in Molecules. A Quantum Theory*; Oxford Science Publications (Clarendon Press): London, 1990.
(17) Popelier, P. L. A. *Atoms in Molecules. An Introduction*; Pearson Education: Harlow, U.K., 2000.
(18) Bader, R. F. W.; Essén, H. *J. Chem. Phys.* **1984**, *80*, 1943.
(19) Popelier, P. L. A.; Bader, R. F. W. *Chem. Phys. Lett.* **1992**, *189*, 542.
(20) Caroll, M. T.; Bader, R. F. W. *Mol. Phys.* **1988**, *65*, 695.
(21) Koch, U.; Popelier, P. L. A. *J. Phys. Chem.* **1995**, *99*, 9747.
(22) Fidanza, N. G.; Suvire, F. D.; Sosa, G. L.; Lobayan, R. M.; Enriz, R. D.; Peruchena, N. M.*THEOCHEM* **2001**, *543*, 185.
(23) Caroll, M. T.; Chang, C.; Bader, R. F. W. *Mol. Phys.* **1988**, *63*, 387.
(24) Sosa, G. L.; Peruchena, N. M.; Contreras, R. H.; Castro, E. A. *THEOCHEM* **1997**, *401*, 77.
(25) Sosa, G. L.; Peruchena, N. M. Contreras, R. H.; and Castro, E. A. *THEOCHEM* **2002**, *577*, 219.
(26) Grimme, S. *J. Am. Chem. Soc.* **1996**, *118*, 1529.
(27) Bader, R. F. W.; Chang, C. *J. Phys. Chem.* **1989**, *93*, 2946.
(28) Bader, R. F. W.; MacDougall, P. J. *J. Am. Chem. Soc.* **1985**, *107*, 6788.
(29) Bader, R. F. W.; Chang, C. *J. Phys. Chem.* **1989**, *93*, 2946.
(30) Caroll, M. T.; Cheeseman, J. R.; Osman, R.; Weinstein, H. *J. Phys. Chem.* **1989**, *93*, 5120.
(31) Werstiuk, N. H.; Laidig, K. E.; *Application of Quantum Theory of Atoms in Molecules to Study of Anomeric Effect in Dimethoxymethane*; ACS Symposium Series 539; American Chemical Society: Washington, DC, 1993.
(32) Bader, R. F. W.; Popelier, P. L. A.; Chang, C. *THEOCHEM* **1992**, *255*, 145.
(33) Niño, A.; Muñoz-Caro, C. *Biophys. Chem.* **2001**, *91*, 49.
(34) Sierraalta, A.; Ruette, F. *J. of Mol. Catal., A: Chem.* **1996**, *109*, 227.
(35) Aray, Y.; Rodriguez, J.; Rivero, J.; Vega, D. *Surf. Sci.* **1999**, *441*, 344.
(36) Popelier, P. L. A. *Coord. Chem. Rev.* **2000**, *197*, 169.
(37) Malcolm, N. O. J.; Popelier, P. L. A. *J. Phys. Chem.* **2001**, *105*, 7638.
(38) Gillespie, R. J. *Struct. Chem.* **1998**, *9*, 73.
(39) Gillespie, R. J. *Can. J. Chem.* **1992**, *70*, 742.
(40) Bader, R. F. W.; Popelier, P. L. A.; Keith, T. A. *Angew. Chem., Int. Ed. Engl.* **1994**, *33*, 620.
(41) Bader, R. F. W.; Gillespie, R. J.; McDougall, P. J. *J. Am. Chem. Soc.* **1988**, *110*, 7329.

(42) Fradera, X.; Austen, M. A.; Bader, R. F. W. *J. Phys. Chem. A* **1999**, *103*, 304.
(43) Bytheway, I.; Gillespie, R. J.; Tang, T. H.; Bader R. F. W. *Inorg. Chem.* **1995**, *34*, 2407.
(44) Gillespie, R. J.; Bytheway, I.; Dewitte, R. S.; Bader, R. F. W. *Inorg. Chem.* **1994**, *33*, 2115.
(45) Bader, R. F. W.; Gillespie, R. J.; Martin, R. J. *Chem. Phys. Lett.* **1998**, *290*, 488.
(46) Bytheway, I.; Popelier, P. L.; Gillespie, R. J. *Can. J. Chem.* **1996**, *74*, 1059.
(47) Bader, R. F. W.; Heard, G. L. *J. Chem. Phys.* **1999**, *111*, 8789
(48) Gillespie, R. J.; Robinson, E. A. *Adv. Mol. Struct. Res.* **1998**, *4*, 1.
(49) Becke A. D.; Edgecombe, K. E. *J. Chem. Phys.* **1990**, *92*, 5397.
(50) Bader, R. F. W.; Johnson, S.; Tang, T. H.; Popelier, P. L. A. *J. Phys. Chem.* **1996**, *100*, 15398.
(51) Gillespie, R. J.; Bayles, D.; Platts, J.; Heard, G. L.; Bader, R. F. W. *J. Phys. Chem. A* **1998**, *102*, 3407.
(52) (a) Coppens, P. *X-ray Charge Densities and Chemical Bonding*; Oxford University Press: New York, 1997. (b) Wilson, K. S. *Nat. Struct. Biol.* **1998**, *5*, 627−630.
(53) Koritsánszky, T.; Flaig, R.; Zobel, D.; Krane, H. G.; Morgenroth, W.; Luger, P. *Science* **1998**, *279*, 356
(54) Frisch, M. J.; Trucks, G. W.; Schlegel, H. B.; Scuseria, G. E.; Robb, M. A.; Cheeseman, J. R.; Zakrzewski, V. G.; Montgomery, J. A., Jr.; Stratmann, R. E.; Burant, J. C.; Dapprich, S.; Millam, J. M.; Daniels, A. D.; Kudin, K. N.; Strain, M. C.; Farkas, O.; Tomasi, J.; Barone, V.; Cossi, M.; Cammi, R.; Mennucci, B.; Pomelli, C.; Adamo, C.; Clifford, S.; Ochterski, J.; Petersson, G. A.; Ayala, P. Y.; Cui, Q.; Morokuma, K.; Malick, D. K.; Rabuck, A. D.; Raghavachari, K.; Foresman, J. B.; Cioslowski, J.; Ortiz, J. V.; Stefanov, B. B.; Liu, G.; Liashenko, A.; Piskorz, P.; Komaromi, I.; Gomperts, R.; Martin, R. L.; Fox, D. J.; Keith, T.; Al-Laham, M. A.; Peng, C. Y.; Nanayakkara, A.; Gonzalez, C.; Challacombe, M.; Gill, P. M. W.; Johnson, B. G.; Chen, W.; Wong, M. W.; Andres, J. L.; Head-Gordon, M.; Replogle, E. S.; Pople, J. A. *Gaussian 98*, revision A.7; Gaussian, Inc.: Pittsburgh, PA, 1998.
(55) Blieger-König, F. W.; Bader, R. F. W.; Tang, T. H. *J. Comput. Chem.* **1982**, *3*, 317.
(56) Bader, R. F. W.; Johnson, S.; Tang, T. H.; Popelier, P. L. A. *J. Phys. Chem.* **1996**, *100*, 15398
(57) Unpublished results from the author rmlb@exa.unne.edu.ar.